Submitted to

XXII International Symposium on Lepton and Photon Interactions, LP2005, June 30, 2005, Uppsala

Abstract: **399**

Session **QCD and hadron structure**

www-h1.desy.de/h1/www/publications/conf/conf_list.html

Diffractive photoproduction of ρ mesons with large momentum transfer at HERA

H1 Collaboration

Abstract

The diffractive photoproduction of ρ mesons with large momentum transfer, $e + p \rightarrow \; e + \rho + Y$, is studied at HERA in the kinematic range $Q^2 < 0.01$ GeV^2, $75 < W < 95$ GeV, $1.5 < |t| < 10.0$ GeV^2 and $M_Y < 5$ GeV. The t dependence of the cross section is measured, as well as the spin density matrix elements. All results are compared to BFKL model predictions.

1 Introduction

The subject of this paper is the study of the photoproduction of ρ mesons at large momentum transfer in high energy ep scattering:

$$e + p \rightarrow e + \rho\ + Y; \quad \rho \rightarrow \pi^+ + \pi^-, \tag{1}$$

where the scattered proton is mainly excited into a system Y of mass M_Y which is much lower than the photon–proton centre of mass energy W ("proton dissociative" scattering). There is also a small contribution from "proton elastic" scattering where the proton remains intact.

For $|t|$ larger than a few GeV^2, t being the square of the four momentum transferred at the proton vertex, perturbative QCD (pQCD) is expected to apply and diffractive ρ production is viewed, in the proton rest frame, as a sequence of three processes well separated in time: the photon fluctuates into a $q\bar{q}$ pair; the $q\bar{q}$ pair is involved in a hard interaction with the proton via the exchange, at lowest order, of two gluons in a colour singlet state and the $q\bar{q}$ pair recombine to form a bound ρ meson. In the leading logarithm approximation the process is represented by the effective exchange of a gluonic ladder, which, in the low x region of interest, is described by BFKL evolution.

The spin density matrix elements are defined as bilinear combinations of the helicity amplitudes $M_{\lambda_\rho \lambda_\gamma}$, where $\lambda_\rho, \lambda_\gamma = -, 0, +$ represent the respective helicities of the ρ meson and the photon [6]. Explicitly they are given by:

$$\begin{aligned}
r^{04}_{00} &= \frac{\langle |M_{+0}|^2 \rangle}{\langle |M_{++}|^2 + |M_{+0}|^2 + |M_{+-}|^2 \rangle} \\
r^{04}_{10} &= \frac{1}{2} \frac{\langle M_{++}M^*_{+0} + M_{+-}M^*_{-0} \rangle}{\langle |M_{++}|^2 + |M_{+0}|^2 + |M_{+-}|^2 \rangle} \\
r^{04}_{1-1} &= \frac{1}{2} \frac{\langle M_{++}M^*_{+-} + M_{+-}M^*_{++} \rangle}{\langle |M_{++}|^2 + |M_{+0}|^2 + |M_{+-}|^2 \rangle}
\end{aligned} \tag{2}$$

In the approximation of s-channel helicity conservation (SCHC), whereby the ρ meson retains the helicity of the photon, both the single-flip and double-flip dependent matrix elements are expected to be zero.

Measurements of high $|t|$ diffractive vector meson photoproduction (ρ, ϕ and J/Ψ) have been performed by the ZEUS collaboration [1] and J/Ψ meson photoproduction at high $|t|$ has also been studied by the H1 Collaboration [2], extending the kinematic range as far as $|t| = 30\ \mathrm{GeV}^2$. The ZEUS measurements of spin density matrix elements for ρ meson production indicate violation of s-channel helicity conservation.

2 Theoretical Model

The process of interest is described by the non-forward BFKL equation for which a complete analytical solution, in the leading logarithm approximation, is presented by Poludniowski *et al.*

in [3, 4]. Their prescription is to factorise the meson production from the hard subprocess using a set of meson wavefunctions expanded on the light-cone. All expansions are performed up to twist-3, i.e. next-to-leading twist, which is the lowest order able to accommodate a non-zero r^{04}_{10} matrix element. The constituent, as opposed to current, quark mass is used to enhance the coupling of the photon to chiral odd $q\bar{q}$ configurations; thereby producing a strong transverse polarisation as supported by previous data [1, 5].

At leading log accuracy there are three free parameters α_s^{IF} (0.21) , α_s^{BFKL} (0.2) and γ (1.0): where α_s^{IF} is the coupling of the two gluons to each impact factor, α_s^{BFKL} is the coupling within the BFKL ladder and γ determines the scale $\Lambda^2 = m_\rho^2 - \gamma t$. The numbers in parenthesis refer to the parameter values chosen to provide the best description of the previous ZEUS measurements [1] and are used to describe the results that follow.

The model of Poludniowski *et al.* predicts violation of SCHC with a hierarchy of helicity amplitudes given by: non-flip (M_{++}) > double-flip (M_{+-}) > single-flip (M_{+0})[1]. These calculations have subsequently been compared to the ZEUS data [1] and, while they provide a reasonable description of the the matrix elements r^{04}_{00} and r^{04}_{1-1}, they are unable to describe the observed small positive value of $\mathrm{Re}\,[\mathrm{r}^{04}_{10}]$.

The theoretical challenge is to provide a simultaneous description of both the t spectra of the vector mesons and the spin density matrix elements; in particular the largeness of the double-flip dependent matrix element r^{04}_{1-1} and the smallness of the single-flip dependent matrix element r^{04}_{00}.

3 Data selection and kinematics

3.1 Event selection

The data used for the present analysis were taken with the H1 detector in the year 2000. The energies of the HERA proton and positron beams were 920 and 27.5 GeV, respectively. The effective luminosity used for the analysis amounts to 20.1 pb^{-1}. The kinematic domain of the measurement is:

$$\begin{array}{rcl} & Q^2 & < 0.01\ \mathrm{GeV}^2 \\ 75 < & W & < 95\ \mathrm{GeV} \\ 1.5 < & |t| & < 10\ \mathrm{GeV}^2 \end{array} \tag{3}$$

where Q^2 is the modulus squared of the four momentum carried by the intermediate photon. The mass of the proton remnant is limited to

$$M_Y < 5\ \mathrm{GeV}. \tag{4}$$

The relevant parts of the detector, for which more details can be found in [7], are the central tracking detector, the liquid argon (LAr) calorimeter and the 44 m electron tagger, a 7×7 unit

[1]There are also the corresponding amplitudes M_{--}, M_{-+} and M_{-0}, which satisfy $M_{--} = M_{++}$, $M_{+-} = M_{-+}$ and $M_{-0} = M_{+0}$.

array of 22 radiation length crystal calorimeters, which detects the scattered positron in the backward direction[2].

The events are triggered by a tagged photoproduction trigger based on the requirement of an energy deposit of greater than 10 GeV in the 44m electron tagger. It also has tracking conditions requiring at least one charged track detected in the central tracker with a transverse momentum larger than 400 MeV along with vertexing requirements. Additionally, there is a veto on the amount of energy deposited in the forward region of the LAr. Events corresponding to reaction (1), in the kinematic range defined by relations (3) are finally selected by requesting:

- the reconstruction of an energy deposit of more than 15 GeV in the 44 m electron tagger (the scattered positron candidate);
- the reconstruction in the central tracking detector of the trajectories of exactly two oppositely charged particles (pion candidates) with polar angles confined within the interval $20^{\mathrm{o}} < \theta < 155^{\mathrm{o}}$. One track is required to have transverse momentum larger than 0.15 GeV and the other larger than 0.45 GeV (to fire the trigger);
- the absence of any signal reconstructed with energy larger than 400 MeV in the LAr calorimeter, which is not associated with the two charged pion candidates. This cut reduces backgrounds due to the production of systems decaying into two charged and additional neutral particles. It also limits the mass of the proton dissociative system to $M_Y \lesssim 5$ GeV;
- events in the mass range $0.6 < M_{\pi\pi} < 1.1$ GeV are selected, while events with $M_{KK} < 1.04$ GeV are discarded, where $M_{\pi\pi}$ and M_{KK} are the invariant mass of the two hadron candidates when considered as pions or kaons respectively (no direct hadron identification is performed for this analysis). The latter cut reduces the background due to diffractive production of ϕ mesons.

The final sample consists, in total, of 2685 events.

3.2 Kinematics and angular distributions

The ρ three-momentum is computed as the sum of the two charged pion candidate momenta. The variable W is calculated using the Jacquet-Blondel method [8]:

$$W^2 \simeq ys, \text{with } y = \frac{E_\rho - p_{z,\rho}}{2E_0}, \tag{5}$$

s being the square of the ep centre of mass energy, E_0 is the incoming positron energy and E_ρ, $p_{z,\rho}$ and $p_{t,\rho}$ being the energy, longitudinal and transverse momentum of the ρ meson, respectively. The variable $|t|$ is determined from the ρ momentum component transverse to the beam direction as

$$|t| \simeq (\vec{p}_{t,\rho})^2 \tag{6}$$

[2]In the H1 convention, the z axis is defined by the colliding beams, the forward direction being that of the outgoing proton beam ($z > 0$) and the backward direction that of the positron beam ($z < 0$).

The measurement of the production and decay angular distributions provides access to the spin density matrix elements. Three angles can be defined: Φ is the angle between the ρ production plane (defined as the plane containing the virtual photon and the ρ directions) and the positron scattering plane in the (γp) centre of mass system, θ^* and ϕ^* are the polar and the azimuthal angles, respectively, of the positively charged decay pion in the ρ rest frame, the quantisation axis being taken as the direction opposite to that of the scattered proton. In this paper, only the distributions of the angles ϕ^* and θ^* are analysed (the angle Φ is not accessible in photoproduction) giving access to the matrix elements r^{04}_{00} and r^{04}_{1-1}.

4 Monte Carlo simulations, backgrounds and systematic errors

4.1 Monte Carlo simulations

A Monte Carlo simulation based on the DIFFVM program [9] is used to describe the proton dissociative production and decay of ρ mesons, and to correct the data for acceptance and smearing effects. The Q^2 and W dependencies of the cross section are taken from the previous measurements [10], while the t dependency is taken according to a power law as measured in the data. The W dependent effects of the 44 m electron tagger are taken into account using the luminosity averaged acceptance curve taken from the data. The M_Y spectrum is parameterised as $\mathrm{d}\sigma/\mathrm{d}M_Y^2 \propto 1/M_Y^{2.15}$ (see [11]).

The simulation includes the angular distributions corresponding to the measurements of the present analysis for the r^{04}_{00} matrix element ($\cos\theta^*$ distribution) and for r^{04}_{1-1} (ϕ^* distribution), while the measurement from [1] is taken for $\mathrm{Re}[\mathrm{r}^{04}_{10}]$. Other angular distributions and correlations are taken in the s-channel helicity conservation (SCHC) approximation.

The mass distribution is described by a relativistic Breit-Wigner distribution, including skewing effects taken from the current analysis. For studies of systematics uncertainties, all simulation parameters have been varied within errors.

The DIFFVM simulation is also used for the description of the ω, ϕ and ρ' backgrounds (see next section). Here the t distributions are taken to have the same parameterisation as for the ρ meson, and the angular distributions are taken isotropic, except for $\phi \to K^+K^-$ [12].

Fig. 1 presents the observed and simulated distributions for several variables of the selected sample of events. They include the amounts of background discussed in section 4.2. Reasonable agreement is observed for all distributions, indicating that the Monte-Carlo simulations can be reliably used to correct the data for acceptance and smearing effects.

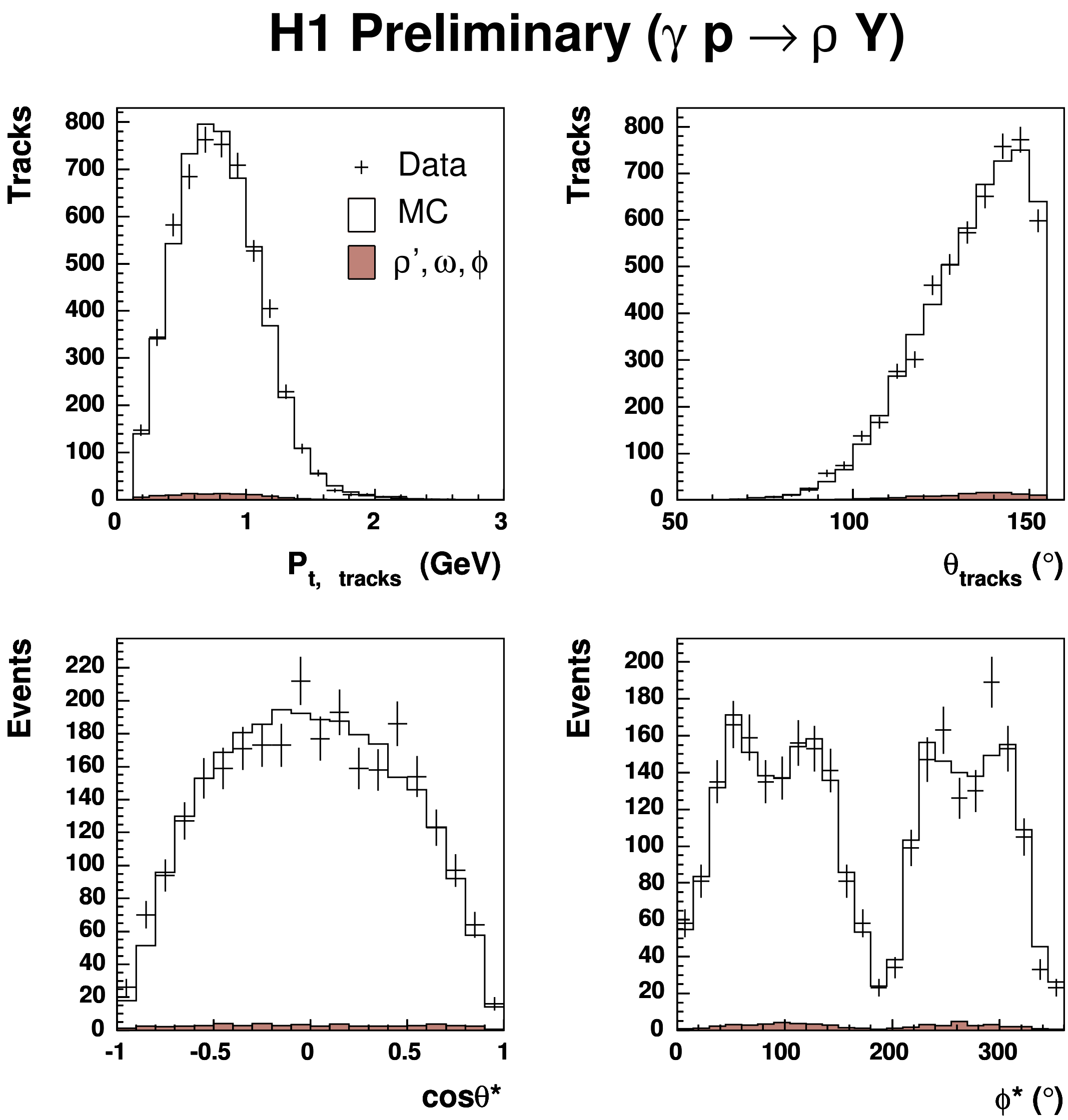

Figure 1: Distribution of the selected events in the kinematic domain (3) for the transverse momentum (a), azimuthal angle of the pion candidates (b), the angular distributions $\cos\theta^*$ (c) and ϕ^* (d). The crosses present the data and the histograms present the Monte-Carlo predictions, including the ω, ϕ and ρ' backgrounds (shaded histogram).

4.2 ω, ϕ and ρ' backgrounds

Diffractive photoproduction of ω, ϕ and ρ' mesons can fake ρ production through the decay channels:

$$\begin{aligned}
&\omega \to \pi^+\pi^-\pi^0, \quad && \omega \to \pi^+\pi^- \\
&\phi \to \pi^+\pi^-\pi^0, \quad && \phi \to K_S^0 K_L^0 \\
&\rho' \to \rho^+\pi^-\pi^0 && \\
&\quad\hookrightarrow \pi^+\pi^0 && (+\, c.c.).
\end{aligned} \tag{7}$$

if the decay photons of the π^0 or the K_L^0 mesons are not detected. This happens in the cases where the energy of the neutral particle is deposited in a crack in the detector, associated to the charged pion tracks, or is smaller than the 400 MeV noise threshold.

The ϕ, ω and ρ' cross sections were taken from measured ratios to the ρ cross section, in the Q^2 range relevant for the analysis: ϕ / $\rho = 0.156$ [1], ω / $\rho = 0.106$ [13] and ρ' / $\rho = 0.2$. In the latter case, the ratio is obtained from the measured ratio $\rho' \to \pi^+\pi^-\pi^+\pi^-$ / $\rho \to \pi^+\pi^- = 0.10 \pm 0.05$ [14, 15] under the assumption

$$\frac{(\rho' \to \rho^+\pi^-\pi^0) + (\rho' \to \rho^-\pi^+\pi^0)}{\rho \to \rho\pi^+\pi^-} = 2. \tag{8}$$

The background contributions in the selected kinematic domain (3) are estimated with the Monte-Carlo simulations, and subtracted from all cross section distributions. They amount to 0.51 %, 0.21 % and 1.30 % for the ω, ϕ and ρ' respectively.

4.3 Systematic errors

The effect of systematic uncertainties affecting the measurements are estimated by varying the event selection and the parameters of the ρ Monte Carlo simulation.

- **Uncertainties on the acceptance and smearing corrections**
  The cross section dependence on t, used to compute acceptances and smearing effects, and to propagate the measurement to fixed values of the kinematical variables, is varied by $\pm$ 0.5 for the power of the t dependence. The modelling of the dissociative proton remnant Y is varied within $(1/M_Y^2)^{\pm 0.3}$. In the case of the angular distributions, the matrix elements r_{00}^{04} and r_{1-1}^{04} are varied by the error obtained from fits to the current data, which is $\pm$ 0.05. The matrix element $\mathrm{Re}[r_{10}^{04}]$ is varied by $\pm$ 0.02, in accordance with the error quoted in [1].

- **Background distributions**
  For dissociative ρ' production, the t dependence is varied by $\pm$ 2.0 for the power of the t slope. The ratios of the background cross sections to the ρ cross section are varied by: $\pm$ 0.02 for ω / ρ, $\pm$ 0.05 for ϕ / ρ, $\pm$ 0.1 for ρ' / ρ.

- **Trigger description**
  The p_t cut of 0.45 GeV, used to restrict the analysis to the region of high trigger efficiency is varied between 0.40 GeV and 0.60 GeV. Further errors coming from re-weighting the trigger efficiency are also taken into account.

- **Tracker description**
  The cut on the θ angle of the reconstructed tracks is varied between $155°$ and $160°$, to estimate the effect of the dependence of the correction factors in that region. The variation of the p_t cut stated above also partially covers the error on the tracker description.

- **Electron tagger description**
  The error on the description of the electron tagger is estimated by varying the acceptance by 3 % as a function of y.

The systematic errors are combined quadratically.

5 Cross sections

In each bin of the kinematical variables, the cross section is computed from the numbers of events in the bin, fully corrected for backgrounds, acceptance and smearing effects using the Monte Carlo simulations described above. At low t, the data are further corrected for the skewing effect obtained for the present data from the Ross-Stodolsky [16] parametrisation. All cross sections presented below, as well as the theoretical model predictions, are normalised to their integrals in the respective kinematic domain.

5.1 $M_{\pi\pi}$ dependence of the cross section

The $M_{\pi\pi}$ dependence of the $\gamma + p \to \rho + Y$ cross section is shown in fig. 2. The superimposed curve shows the result of a fit to a relativistic Breit-Wigner with Ross-Stodolsky skewing, for which $\chi^2/ndf = 17.12/16$. The resulting values for the ρ mass and width, which are $M_\rho = 0.771 \pm 0.007$ GeV and $\Gamma_\rho = 0.180 \pm 0.029$ GeV respectively, are compatible with the PDG values [17]. The overall value of the skewing parameter n is consistent with zero.

5.2 t dependence of the cross section

The t dependence of the $\gamma + p \to \rho + Y$ cross section is presented in Fig. 3. The dependence is well described by the BFKL model of Poludniowski *et al.* Further, it can be fitted by a power law distribution of the form $d\sigma/dt \propto |t|^{-n}$, where $n = 4.41 \pm 0.07\,(\mathrm{stat.})\,^{+0.07}_{-0.05}\,(\mathrm{syst.})$, over the measured range of t.

The ZEUS collaboration [1] obtained a power law of $n = 3.21 \pm 0.04\,(\mathrm{stat.}) \pm 0.15\,(\mathrm{syst.})$ for the kinematic range $Q^2 < 0.02\ \mathrm{GeV}^2$, $80 < W < 120$ GeV, $1.1 < |t| < 10.0\ \mathrm{GeV}^2$ and $M_Y < 25\ \mathrm{GeV}$, which is also well described by theory, and is understood to be shallower than the value measured here due to the different M_Y range.

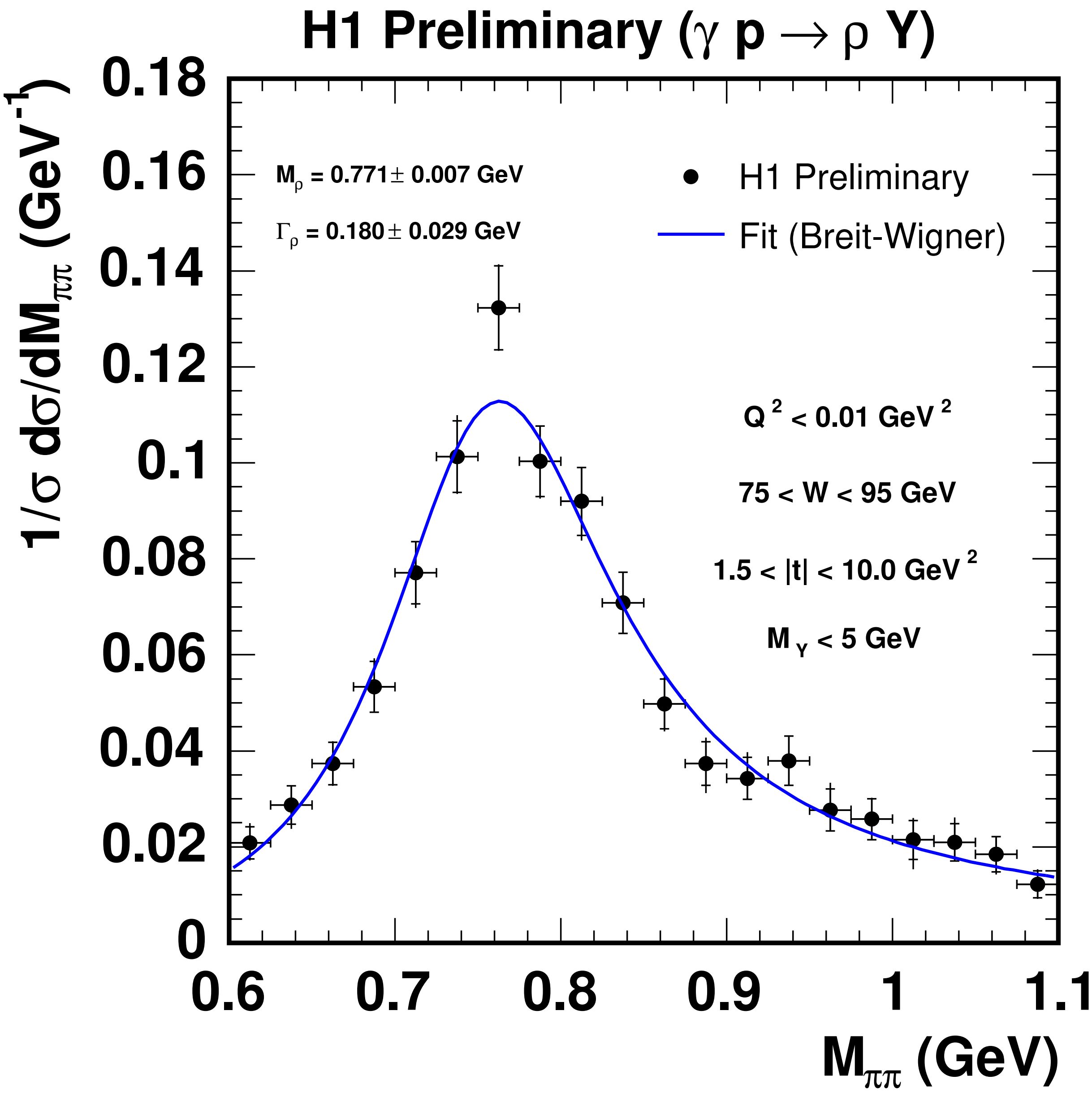

Figure 2: The $M_{\pi\pi}$ dependence of the $\gamma + p \to \rho + Y$ cross section. The inner error bars show the statistical errors, while the outer ones represent the sum of the statistical and non-correlated systematic errors added in quadrature. The superimposed curve shows the result of a fit to a relativistic Breit-Wigner with Ross-Stodolsky skewing.

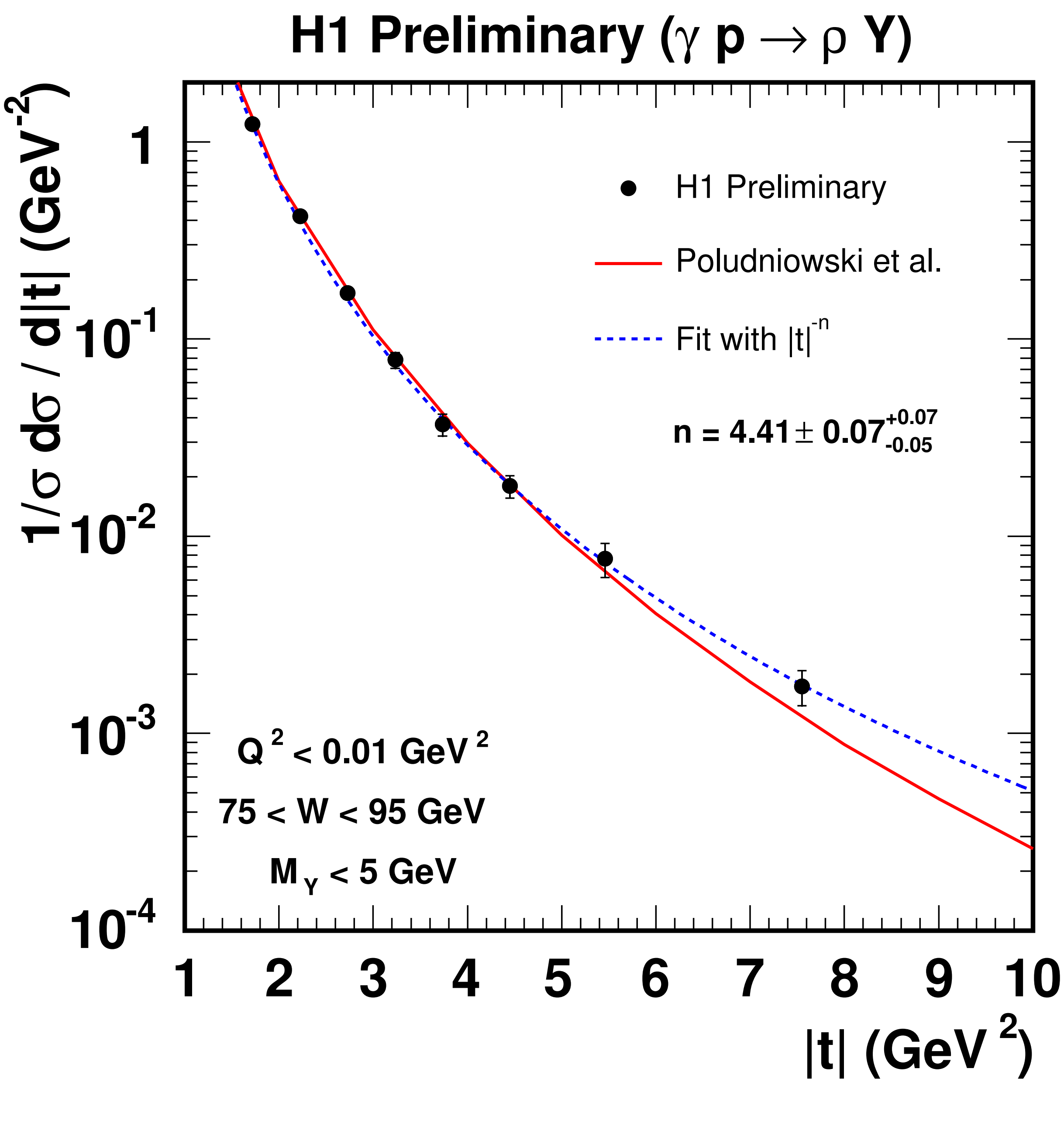

Figure 3: The t dependence of the $\gamma + p \rightarrow \rho + Y$ cross section. The inner error bars show the statistical errors, while the outer ones represent the sum of the statistical and non-correlated systematic errors added in quadrature. The dashed line is the result of a fit to a power law distribution $|t|^{-n}$, which results in a power $n = 4.41 \pm 0.07\,(\mathrm{stat.})\,^{+0.07}_{-0.05}\,(\mathrm{syst.})$. The full line shows the result from the BFKL model of Poludniowski *et al.*

5.3 r^{04}_{00} spin density matrix element

Fig. 4 presents the $\cos\theta^*$ dependence of the $\gamma + p \to \rho + Y$ cross section, for three intervals in $|t|$. The superimposed curves show results of fits of the form

$$\frac{\mathrm{d}\sigma}{\mathrm{d}\cos\theta^*} \propto 1 - r^{04}_{00} + (3\, r^{04}_{00} - 1)\cos^2\theta^*, \tag{9}$$

along with the expectation from SCHC. The extracted values of the r^{04}_{00} spin density matrix element are shown as a function of $|t|$ in fig. 6. Also shown are the results of the ZEUS Collaboration [1], with which there is excellent agreement. The results are close to zero, indicating that the production is dominated by transversely polarised ρ mesons. The BFKL Model of Poludniowski *et al.* also correctly describes the small values of r^{04}_{00}.

5.4 r^{04}_{1-1} spin density matrix element

Fig. 5 presents the ϕ^* dependence of the $\gamma + p \to \rho + Y$ cross section, for three intervals in $|t|$. The superimposed curves show results of fits of the form

$$\frac{\mathrm{d}\sigma}{\mathrm{d}\phi^*} \propto 1 - 2r^{04}_{1-1}\ \cos 2\phi^* \tag{10}$$

along with the expectation from SCHC. The extracted values of the r^{04}_{1-1} spin density matrix element are shown as a function of $|t|$ in fig. 6. Also shown are the results of the ZEUS Collaboration [1], with which there is excellent agreement. Values significantly different from zero are obtained for the r^{04}_{1-1} matrix element, confirming s-channel helicity non-conservation [1, 5, 18, 19]. The prediction arising form the BFKL model of Poludniowski *et al.* for r^{04}_{1-1}, although qualitatively able to reproduce the data, is too large at low values of $|t|$.

6 Conclusions

The diffractive photoproduction of ρ mesons, $e + p \to e + \rho + Y$, has been studied using the H1 detector at HERA in the kinematic range $Q^2 < 0.01$ GeV^2, $75 < W < 95$ GeV, $1.5 < |t| < 10$ GeV^2 and $M_Y < 5$ GeV. The t dependence of the γp cross section is measured and fitted with a power law of the form $|t|^{-n}$, which results in $n = 4.41 \pm 0.07\ (\mathrm{stat.})\ ^{+0.07}_{-0.05}\ (\mathrm{syst.})$. Moreover, it is well described by BFKL model predictions. The spin density matrix elements r^{04}_{00} and r^{04}_{1-1} are measured as a function of t. The r^{04}_{00} matrix element is consistent with zero while the r^{04}_{1-1} matrix element differs significantly from zero and thus confirms violation of SCHC [1, 5, 18, 19]. BFKL model predictions describe r^{04}_{00} well but the prediction for r^{04}_{1-1}, although qualitatively able to reproduce the data, is too large at low $|t|$.

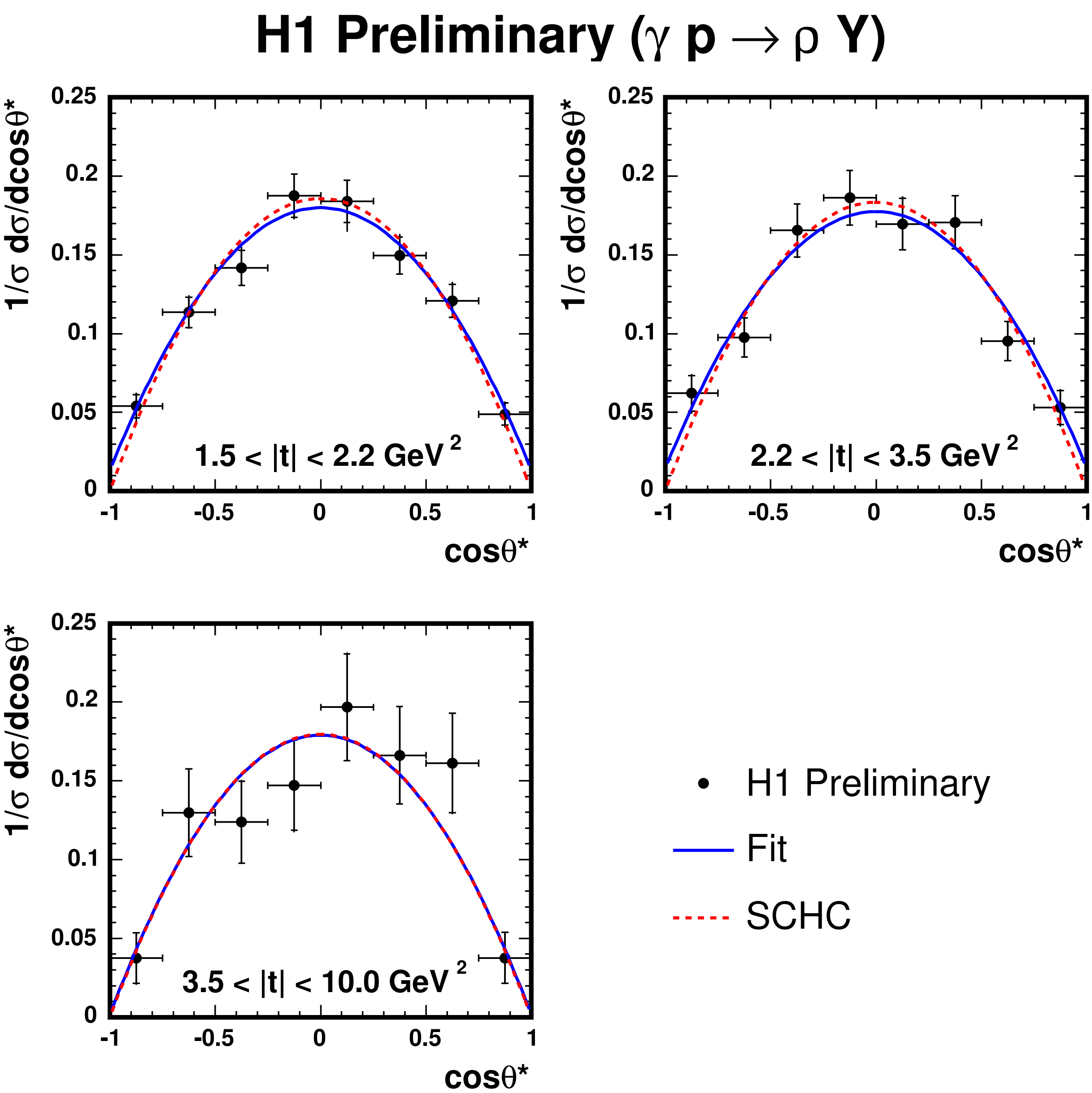

Figure 4: The $\cos\theta^*$ dependence of the $\gamma + p \rightarrow \rho + Y$ cross section, for three $|t|$ intervals. The inner error bars show the statistical errors, while the outer ones represent the sum of the statistical and non-correlated systematic errors added in quadrature. The superimposed curves show the results of fits to the relation 9 (solid) and the predictions of SCHC (dashed)

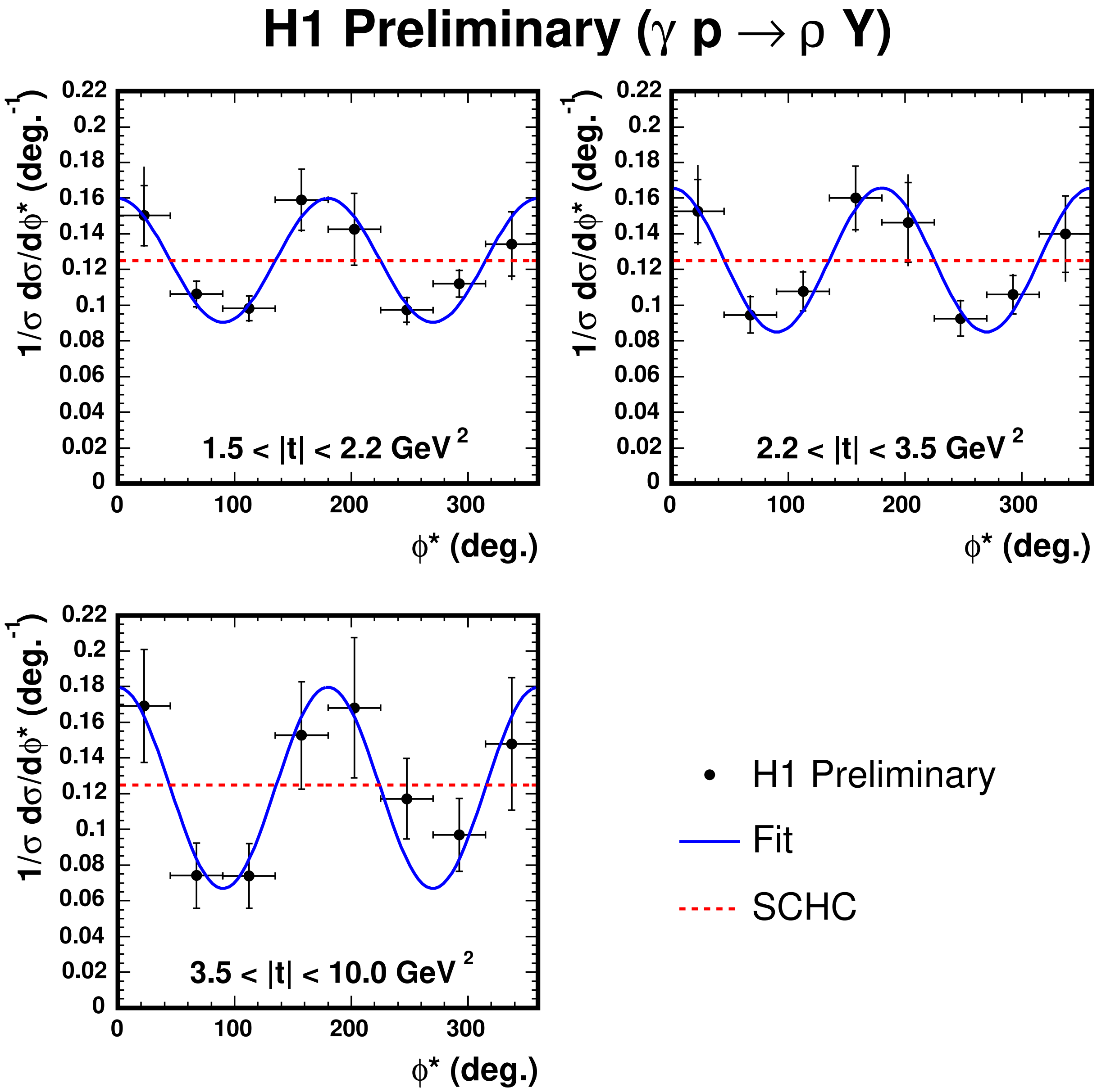

Figure 5: The ϕ^* dependence of the $\gamma + p \rightarrow \rho + Y$ cross section, for three $|t|$ intervals. The inner error bars show the statistical errors, while the outer ones represent the sum of the statistical and non-correlated systematic errors added in quadrature. The superimposed curves show the results of fits to the relation 10 (solid) and the predictions of SCHC (dashed)

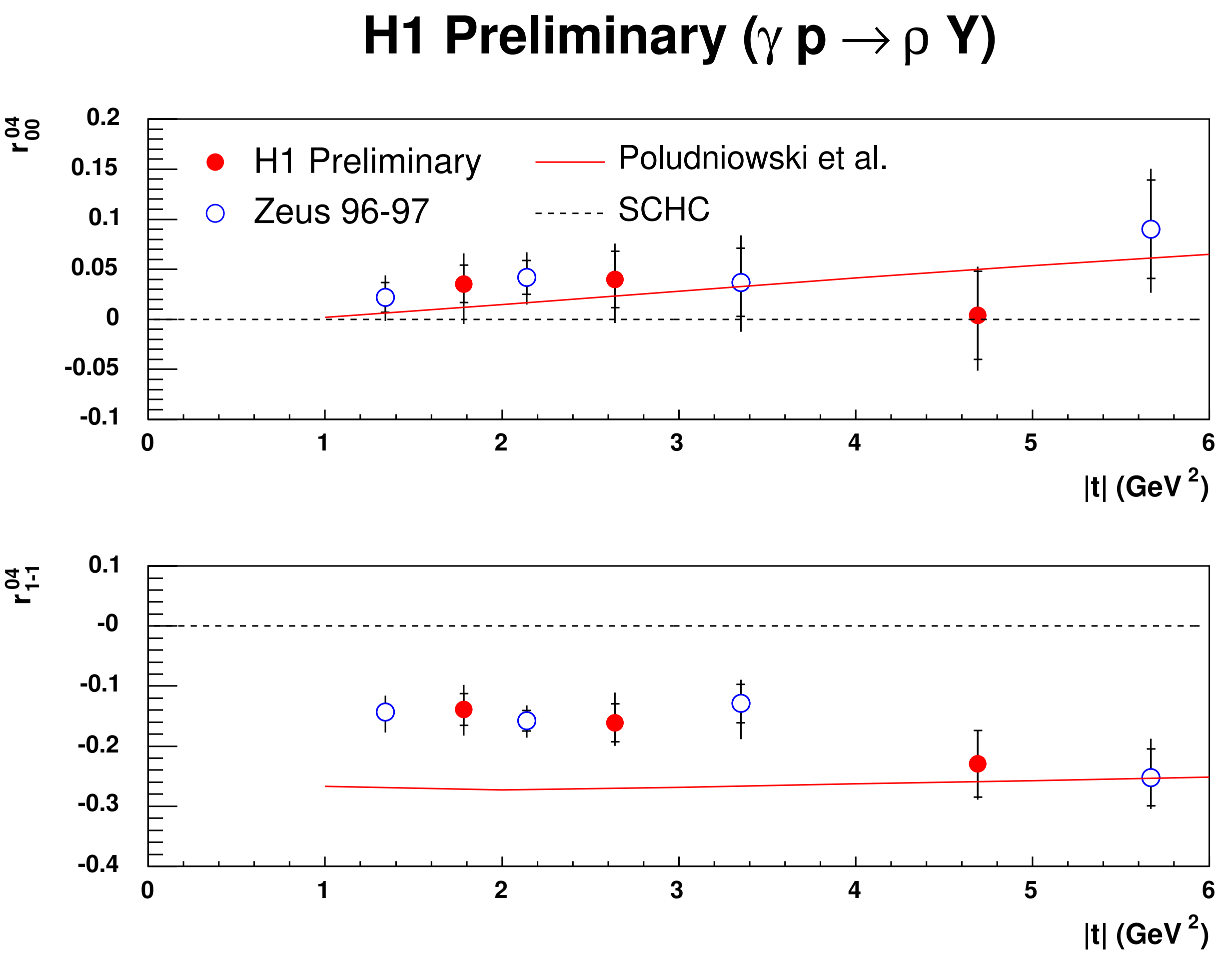

Figure 6: Measurements of the r^{04}_{00} and r^{04}_{1-1} spin density matrix elements as a function of $|t|$ (full points) together with ZEUS previous measurements [1] (open points). The inner error bars show the statistical errors, while the outer ones represent the sum of the statistical and systematic errors added in quadrature. The full lines show the results from the BFKL model of Poludniowski *et al.*, while the dashed lines show the prediction from SCHC

Acknowledgements

We are grateful to the HERA machine group whose outstanding efforts have made and continue to make this experiment possible. We thank the engineers and technicians for their work in constructing and now maintaining the H1 detector, our funding agencies for financial support, the DESY technical staff for continual assistance, and the DESY directorate for the hospitality which they extend to the non DESY members of the collaboration. We would also like to thank J. Forshaw and R. Enberg for providing the theoretical model calculations used throughout.

References

[1] S. Chekanov *et al.* [ZEUS Collaboration], Eur. Phys. J. **C26** (2003) 389 [hep-ex/0205081].

[2] A. Aktas *et al.* [H1 Collaboration], Phys. Lett. B **568** (2003) 205 [hep-ex/0306013].

[3] R. Enberg *et al.*, JHEP **309** (2003) 008 [hep-ph/0306232].

[4] G. G. Poludniowski *et al.*, JHEP **312** (2003) 002 [hep-ph/0311017].

[5] C. Adloff *et al.* [H1 Collaboration], Phys. Lett. **B539** (2002) 25 [hep-ex/0203022].

[6] K. Schilling and G. Wolf, Nucl. Phys. **B61** (1973) 381-413.

[7] I. Abt *et al.* [H1 Collaboration], Nucl. Instr. Meth. **A386** (1997) 310 and 348.

[8] F. Jacquet and A. Blondel, DESY 79-048 (1979) 377.

[9] B. List and A. Mastroberardino, in Proc. of the Workshop on Monte Carlo Generators for HERA Physics, A.T. Doyle et al. ed., DESY-PROC-1999-02 (1999) 396.

[10] X. Janssen [H1 Collaboration], Acta Phys. Polon. B **33** (2002) 3529 [hep-ex/0207011].

[11] K. Goulianos, Phys. Rep. **101** (1983) 169.

[12] C. Adloff *et al.* [H1 Collaboration], Phys. Lett. **B483** (2000) 360 [hep-ex/0005010].

[13] J. Breitweg *et al.*, Phys. Lett. **B487** (2000) 273 [hep-ex/0006013].

[14] W. D. Shambroom *et al.*, Phys. Rev. **D26** (1982) 1.

[15] T. Killian *et al.*, Phys. Rev. **D21** (1980) 3005.

[16] M. Ross and L. Stodolsky, Phys. Rev. **149** (1966) 1173.

[17] S. Eidelman *et al.* [Particle Data Group], Phys. Lett. **B592** (2004) 1.

[18] C. Adloff *et al.* [H1 Collaboration], Eur. Phys. J. **C13** (2000) 371 [hep-ex/9902019].

[19] J.Breitweg *et al* [Zeus Collaboration], Eur. Phys. J. **C14** (2000) 2, 213-238 [hep-ex/9910038].